ELSEVIER

Contents lists available at ScienceDirect

Journal of the European Ceramic Society

journal homepage: www.elsevier.com/locate/jeurceramsoc





Orientation-dependent, field-induced phase transitions in soft lead zirconate titanate piezoceramics

Jianwei Zhao, Stephen D. Funni, Emily R. Molina, Elizabeth C. Dickey, Jacob L. Jones *

Department of Materials Science and Engineering, North Carolina State University, Raleigh, NC, United States

ARTICLE INFO

Keywords:
PZT piezoceramics
In situ high-energy XRD
Orientation-dependent phase transitions

ABSTRACT

In situ high-energy X-ray diffraction (XRD) was performed on lead-zirconate-titanate-based ferroelectric materials with composition near the morphotropic phase boundary (MPB). The utilization of the two-dimensional area detector in *in situ* field-dependent experiments enables the complete analysis of the material response with respect to all azimuthal angles at each field amplitude. The studies reveal that the field-induced phase transition from tetragonal to rhombohedral is dependent on crystal orientation in Nb-doped PbZr $_{0.50}$ Ti $_{0.50}$ O $_{3}$, which is further in composition from the MPB. This synchrotron-based XRD characterization approach illustrates the importance in evaluating the orientation-dependence of phase transitions in piezoelectric and ferroelectric polycrystalline materials.

1. Introduction

Lead zirconate titanate (Pb $Zr_xTi_{1-x}O_3$, 0 < x < 1), or PZT, based materials exhibit excellent piezoelectric and ferroelectric properties, especially for compositions near the morphotropic phase boundary (MPB). Two main mechanisms are often considered to be the origin of high electric-field-induced strain in PZT-based materials [1,2]: (1) an intrinsic contribution that results from the field-induced lattice distortion [2,3] and (2) an extrinsic contribution that originates from other factors such as domain wall motion and interphase boundary motion [4-6]. For PZT-based materials with compositions near the MPB ($x\sim0.52$), electric-field-induced phase transitions can occur between co-existing phases or phases near the limit of their stability. For example, field-induced changes to phase fractions have been observed in PZT compositions containing both tetragonal (P4mm) and monoclinic (Cm) phases [7] or tetragonal (P4mm) and rhombohedral (R3m) phases [8]. Generally, field-induced phase changes can occur abruptly and completely with field application, e.g. as shown in lithium-doped K_{0.5}Na_{0.5}NbO₃ [9], or as gradual changes in phase fraction with applied electric field in lead-based materials [7,10,11]. The nature of these phase changes is central to understanding the origins of the macroscopic properties including the field-induced strain. In ferroelectric single crystals, electric field-induced phase transitions can occur preferentially when electric fields are applied parallel to specific crystallographic directions. For example, <001>-cut Pb(Mg_{1/3}Nb_{2/3})O₃-PbTiO₃ and Pb(Zn_{1/3}Nb_{2/3})O₃-PbTiO₃ single crystals exhibit ultrahigh field-induced strains due to phase transitions, whereas <111>-cut single crystals do not exhibit phase transitions and, therefore, exhibit inferior field-induced strains and piezoelectric properties [12,13]. Here, we extend this idea to ferroelectric polycrystalline materials and posit that electric-field-induced phase transitions can be orientation-dependent in piezoceramics. This means that phase transitions may be favored in some crystallographic orientations over other orientations and, as a result, the overall piezoceramic may exhibit a partial phase transition.

For decades, *in situ* X-ray diffraction (XRD) with applied electric fields has served as a powerful approach to probe the important and coupled roles of lattice distortions, ferroelectric/ferroelastic domain wall motion, and phase transitions to macroscopic properties such as field-induced strain in polycrystalline ferroelectric materials [7,9–11]. In the simplest construction, a laboratory-scale powder diffractometer can be used in conjunction with an *in situ* electric field cell in which electrodes are typically applied to opposing faces of the sample [8]. Experiments conducted in Bragg-Brentano geometry with the electrode surfaces parallel to the Bragg plane are only sensitive to scattering vectors parallel to the electric field direction. The diffraction data therefore provide information about the lattice strains and preferred orientation (*i.e.*, domain fraction changes) only in the direction parallel

E-mail address: jacobjones@ncsu.edu (J.L. Jones).

 $^{^{\}ast}$ Corresponding author.

to the electric field.

As demonstrated by Jones *et al.*, the preferred orientation induced by ferroelectric/ferroelastic domain wall motion produces a type of crystallographic texture that often necessitates a more rigorous texture characterization approach [14]. Most of the polycrystalline samples investigated via these techniques are initially randomly oriented and exhibit an electric-field-induced fiber symmetry after electrical poling (*i. e.*, transversely isotropic). To completely describe the texture, an entire orientation distribution function (ODF) that describes the relative probability of all crystallographic orientations in 3-dimensional (3D) Euler space can be calculated [15–17]. However, due to sample symmetry, it is not necessary to calculate an entire ODF. At minimum, however, characterizing texture in these materials often relies on integrating more information than is available in a single diffraction pattern representing a single scattering vector.

A more rigorous and increasingly common approach for robust texture quantification is to use a 2-dimensional (2D) area detector in transmission geometry [18], as illustrated in Fig. 1. This method is most readily employed at a synchrotron source, where high-energy X-rays can be utilized to penetrate through sample thicknesses of 100 μ m to 1 mm. This geometry enables the characterization of pole figures that exhibit fiber or uniaxial symmetry by evaluating the Bragg peak intensities as a function of azimuthal direction (φ), i.e., the change in intensity and scattering angle relative to the electric field direction.

In this work, we demonstrate the value of using this experimental approach to simultaneously characterize the anisotropy in field-induced intrinsic strain, domain wall motion, and orientation-dependent phase transitions in ferroelectric polycrystalline materials. Specifically, we investigate a ferroelectric PZT composition near the MPB that is initially in a single tetragonal phase, but changes into co-existing tetragonal and rhombohedral phases during electric field application which remain after release of the field. In addition, we elucidate the role of crystal orientation on the phase transition process, demonstrating its anisotropy. We compare the response of the MPB composition to a tetragonal-phase composition further from the MPB. The results demonstrate that complete analysis of orientation-dependent diffraction data provides new insight into the crystal anisotropy of field-induced phase transitions in polycrystalline ferroelectrics.

2. Materials and methods

The synchrotron-based, *in situ* high-energy XRD with applied electric fields was carried out in beamline 11-ID-C at the Advanced Photon Source (APS) at Argonne National Laboratory. The X-ray beam had an

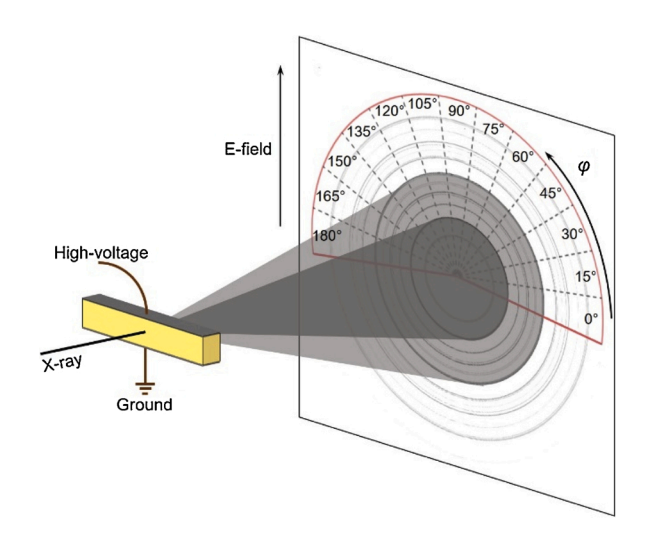


Fig. 1. Schematic of the synchrotron-based experimental setup at beamline 11-ID-C, APS, with definition of azimuthal angle, φ .

energy of 105.7 keV (wavelength of 0.1173 Å) and a beam size of 500 $\mu m \times 500 \mu m$, which can penetrate mm-scale ceramic bars for transmission geometry experiments. The piezoceramics were PZT with 1% niobium-doping; specific compositions including Nb-PbZr_{0.50}Ti_{0.50}O_3 (Nb-PZT 50/50) and Nb-PbZr_{0.53}Ti_{0.47}O_3 (Nb-PZT 53/47), were provided by PI Ceramic (PI Ceramic GmbH, Lederhose, Thuringia, Germany). Both materials have a similar coercive field of $\sim \! 1$ kV/mm. The pellets were fabricated under the project from Ref. [19] where both Nb-PZT 50/50 and 53/47 are single tetragonal phase in the virgin (electrically unpoled) state [20]. According to Ref. [19], Nb-PZT 50/50 has a d_{33} in the poled state of 291 pm/V, whereas Nb-PZT 53/47 has a d_{33} in the poled state of 526 pm/V. From grain size distribution measurements in Ref. [19], it was determined that there was no significant difference in grain size between these two compositions and the mean grain size was approximately 6 μm .

Rectangular bars of dimension 5 mm x 1 mm x 1 mm were cut from the monolithic Nb-PZT pellets and painted with silver paste on two opposing parallel 5 mm x 1 mm surfaces. The bar was placed on a customized sample stage for application of electric fields via a high-voltage amplifier (AMS-10B2, Matsusada Precision, Shiga-ken, Japan) that was driven by a wavefunction generator (Agilent 33220A, Keysight Technologies, Santa Rosa, CA). Unipolar electric fields were applied to the specimens using steps of 1 kV/mm and up to 3 kV/mm maximum. 2D Debye-Scherrer patterns were measured on a PerkinElmer area detector in the transmission geometry.

Data reduction was performed using the open-source software Fit2D [21]. The obtained 2D Debye-Scherrer rings were divided into sectors as a function of azimuthal angle (φ) with respect to the sample geometry, where each sector had an integration width of 15°. Data from all individual 13 sectors were evaluated in the present work. As illustrated in Fig. 1, the 90° sector is parallel to the electric field direction and contains scattering information from scattering vectors oriented approximately parallel to the electric field. The 0° and 180° sectors are horizontal and contain information from scattering vectors perpendicular to the electric field direction.

3. Results

Fig. 2 shows the tetragonal phase 002 and 200 reflections (herein referred to as $002_{\rm T}$ and $200_{\rm T}$) as a function of azimuthal angle for Nb-PZT 50/50, which is the composition far from the MPB. As seen from Fig. 2(a), at the virgin state, $002_{\rm T}$ and $200_{\rm T}$ reflection intensities are nearly constant with respect to azimuthal angle, with the $200_{\rm T}$ reflection approximately twice as intense as the $002_{\rm T}$ consistent with the tetragonal crystal symmetry. However, at the maximum electric field amplitude as plotted in Fig. 2(b), the relative $002_{\rm T}$ and $200_{\rm T}$ reflection intensities vary as a function of azimuthal angle. For example, along the electric field direction ($\varphi=90^\circ$) the $200_{\rm T}$ reflection intensity is suppressed while the $002_{\rm T}$ reflection intensity is enhanced, which is a signature of ferroelectric/ferroelastic domain wall motion [14].

Fig. 3 shows peak intensities as a function of azimuthal angle for Nb-PZT 53/47, the composition closer to the MPB, in the virgin state and at maximum electric field. The figure shows that, in the virgin state, Nb-PZT 53/47 has well-separated 002_T and 200_T reflections in all azimuthal angles. However, with an applied electric field of 3 kV/mm, an additional peak appears between the 002_T and 200_T reflections at approximately the 45° and 135° azimuthal angles, which indicates that a new phase emerges under the field application. Due to Nb-PZT 53/47 having a composition close to the MPB, a composition in which tetragonal and rhombohedral phases have been shown to coexist, the emerged peak can be ascribed to the 200 reflection in the rhombohedral phase, 200_R. Although the data from the Nb-PZT 53/47 sample exhibits evidence of a transition to the rhombohedral phase under application of an electric field at approximately the 45° and 135° azimuthal angles, the other azimuthal angles do not show a new peak emerging. Instead, the other angles evidence a stable tetragonal phase with domain wall

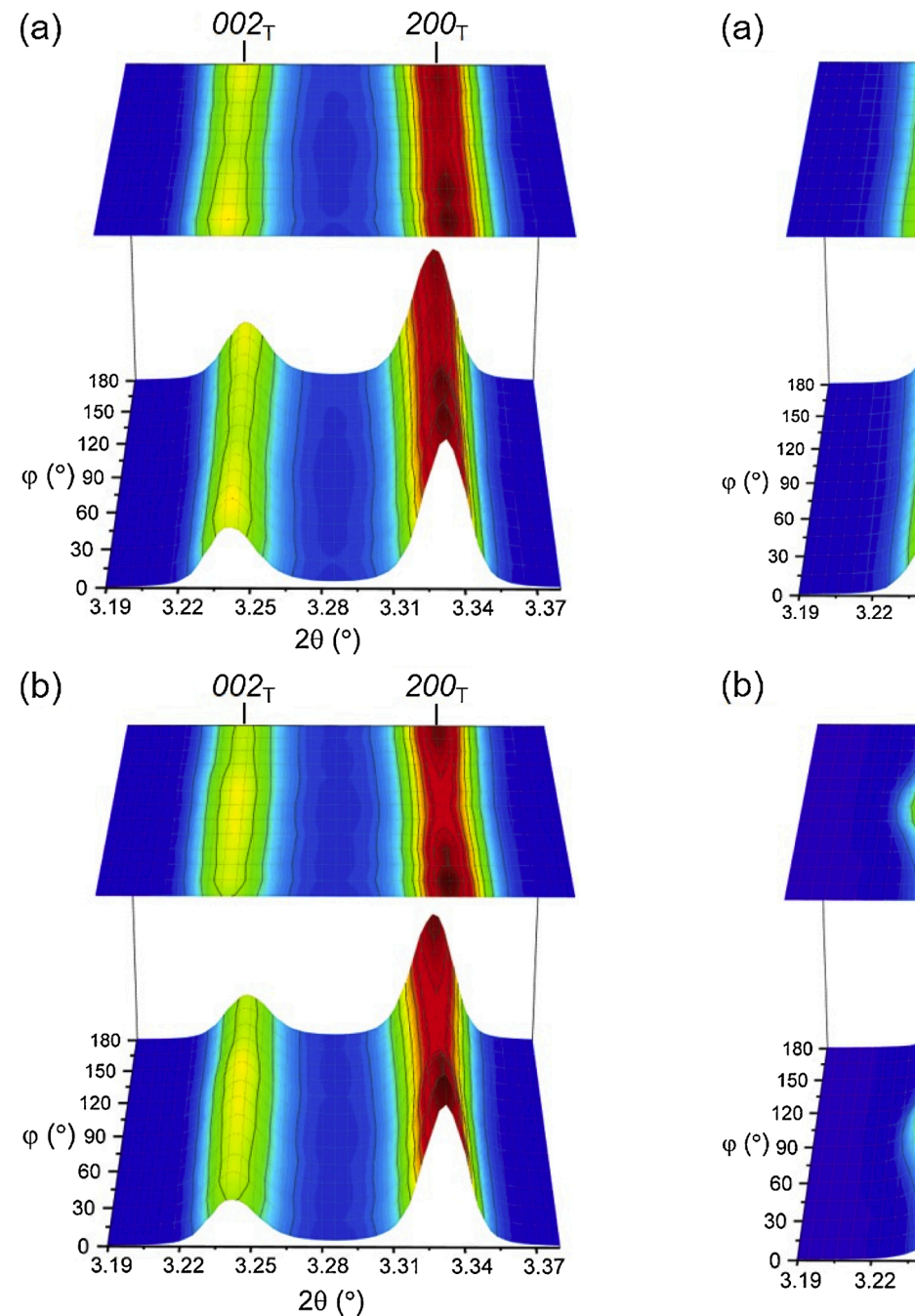


Fig. 2. Peak intensities as a function of azimuthal angle, ϕ , for Nb-PZT 50/50 at (a) the virgin state and (b) 3 kV/mm.

motion, which is apparent from the $002_{\rm T}$ and $200_{\rm T}$ reflection intensity interchanges and lack of appearance of an additional peak. It is worth noting that, in the cases where phase transitions occur from tetragonal (P4mm) to rhombohedral (R3m), the tetragonal phase 111 reflection (referred to as $111_{\rm T}$) is expected to split into rhombohedral phase 111 and $11\overline{1}$ reflections (referred to as $111_{\rm R}$ and $11\overline{1}_{\rm R}$). However, for the Nb-PZT 53/47 sample, the split of the 111 peak is not observed along the 45° and 135° azimuthal angles, as presented in the Supplementary Information. One of the reasons is that, even with phase transitions, the tetragonal phase fraction still dominates the phase composition, which hinders the observation of the 111 peak split. Additionally, the XRD setup utilized at beamline 11-ID-C (high energy with 2D detector, which is ideal for penetrating through bulk polycrystalline materials) may not have high enough resolution to see the peak split, i.e., unable to resolve

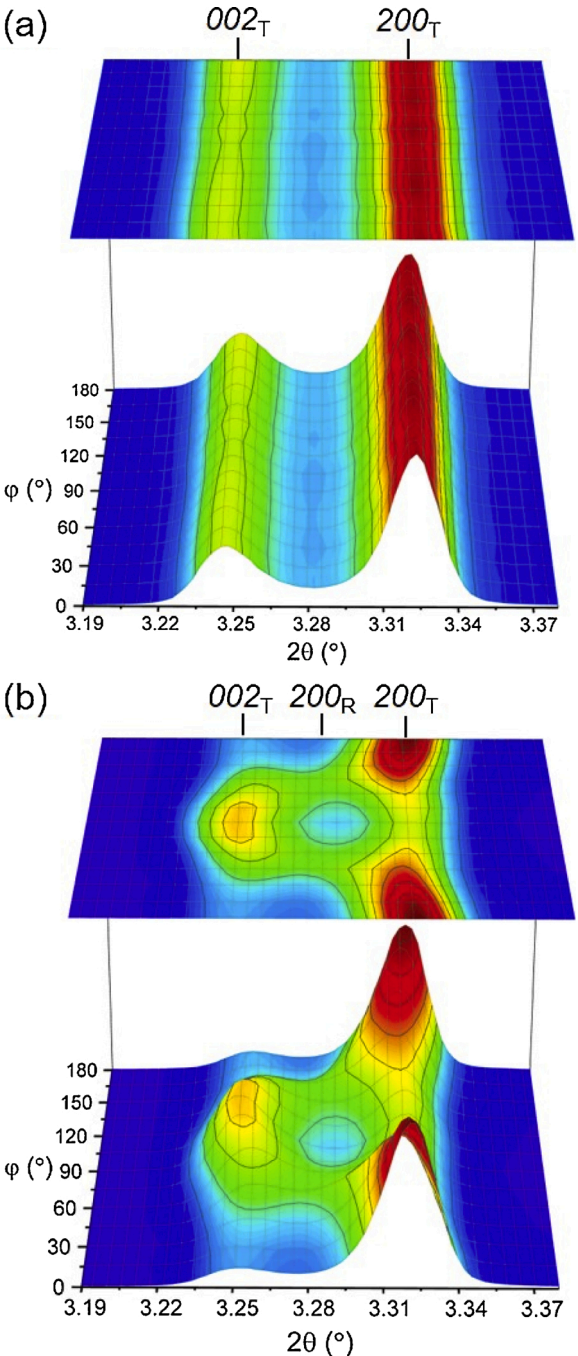


Fig. 3. Peak intensities as a function of azimuthal angle, ϕ , for Nb-PZT 53/47 at (a) the virgin state and (b) 3 kV/mm.

the splitting of 111_R and $11\overline{1}_R$ reflections.

The degree of preferred orientation of domains, or 002 domain texture strength, can be calculated using the intensities of the 002_T and 200_T reflections in any state relative to the intensities in an untextured state according to the equation [14]:

$$f_{002} (\text{mrd}) = 3 \frac{R_{002}}{R_{002} + 2R_{200}}$$
 (1)

where, R_{hkl} is the ratio of integrated intensity of reflection hkl at an electric field to the integrated intensity of the reflection in the unpoled state. By using Eq. (1), the 002 domain texture strength is calculated at all azimuthal angles in terms of multiples of a random distribution (mrd). Fig. 4 presents the computed 002 domain texture strength in both

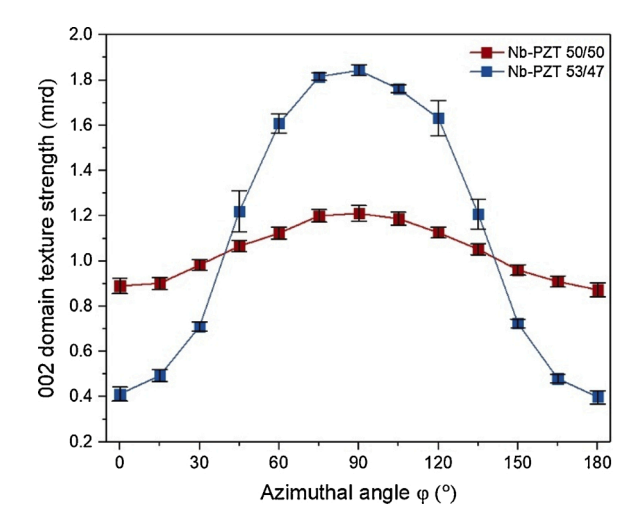


Fig. 4. At 3 kV/mm, the 002 domain texture strength in Nb-PZT 50/50 and Nb-PZT 53/47 as a function of azimuthal angle.

compositions as a function of azimuthal angle at maximum 3 kV/mm. For both compositions, the strongest texture strength is observed along the 90° azimuthal angle, which is parallel to the electric field direction. In comparison with Nb-PZT 50/50 exhibiting maximum $f_{002}=1.21$ mrd, Nb-PZT 53/47 exhibits a maximum $f_{002}=1.84$ mrd parallel to the field direction, which suggests more extensive domain wall motion in the tetragonal phase in compositions nearest the MPB.

4. Discussion

In some prior work, an assumption has been made that the sectors representing "45 degrees away from the field direction" (e.g., azimuthal angles of 45° and 135° in Fig. 1) contain texture-free information that can be used for phase fraction calculations and crystal structure refinements, e.g., through the Rietveld method [7,22,23]. This approach assumes that the phase transition is independent of the electric field orientation. In the present work, however, we demonstrate that the tetragonal-to-rhombohedral phase transition is anisotropic, with

rhombohedral-phase peaks observed in the sectors that are 45° from the electric field direction and not in other azimuthal sectors.

Fig. 5 schematically illustrates the orientation-dependent phase transition mechanism in Nb-PZT 53/47. As a polycrystalline piezoceramic, the grains and ferroelectric domains are initially oriented in all possible crystallographic orientations equally, i.e., collectively representing a random orientation. The hexagons represent grains in the sample with non-180° domain walls (dashed lines) separating the adjacent ferroelectric/ferroelastic striped domains. Note that each grain contains multiple domains, which is expected since the mean grain size of these materials is $6 \mu m$. Two of these orientations are shown in Fig. 5, one that represents a crystallographic orientation with [001] oriented parallel (Fig. 5(a, c)), and the other orientation with the [001] oriented at approximately 45° to the applied electric field (Fig. 5(b, d)). In the unpoled state, Fig. 5(a-b), both orientations are in the tetragonal phase. With an applied electric field (Fig. 5(c-d)), unit cells in these two orientations are driven to elongate parallel to the macroscopic field direction due to the overall longitudinal piezoelectric distortion of the sample. As illustrated in Fig. 5(c), the [001] oriented grain can elongate parallel to the field direction through the process of domain wall motion. On the other hand, for other crystal orientations, such as a grain with [111] oriented parallel to the field direction (represented in the 2D grain in Fig. 5(b) as the [110] direction parallel to the field direction), this distortion can be better accommodated by a phase transition to a rhombohedral-like phase (Fig. 5(d)). The illustrations in Fig. 5 are simplified 2D examples of a more complex 3D material response but illustrate why the phase transition may occur selectively in some crystal orientations but not throughout all orientations in the polycrystalline aggregate.

To further understand the orientation-dependent response, we evaluate electric-field-induced lattice strains of the tetragonal phase. Fig. 6 shows the orientation-dependent electric field-induced lattice strains that are parallel to the field direction in both tetragonal phase compositions (Nb-PZT 50/50 and Nb-PZT 53/47) during an applied electric field of 3 kV/mm. Only the 90° azimuthal sector, which is parallel to the electric field direction, is used in this strain analysis approach, which is adopted from prior studies [6,24]. The radial magnitude in the polar plot represents the amplitude of field-induced lattice strain. The data point for (002) represents 002 lattice strains in

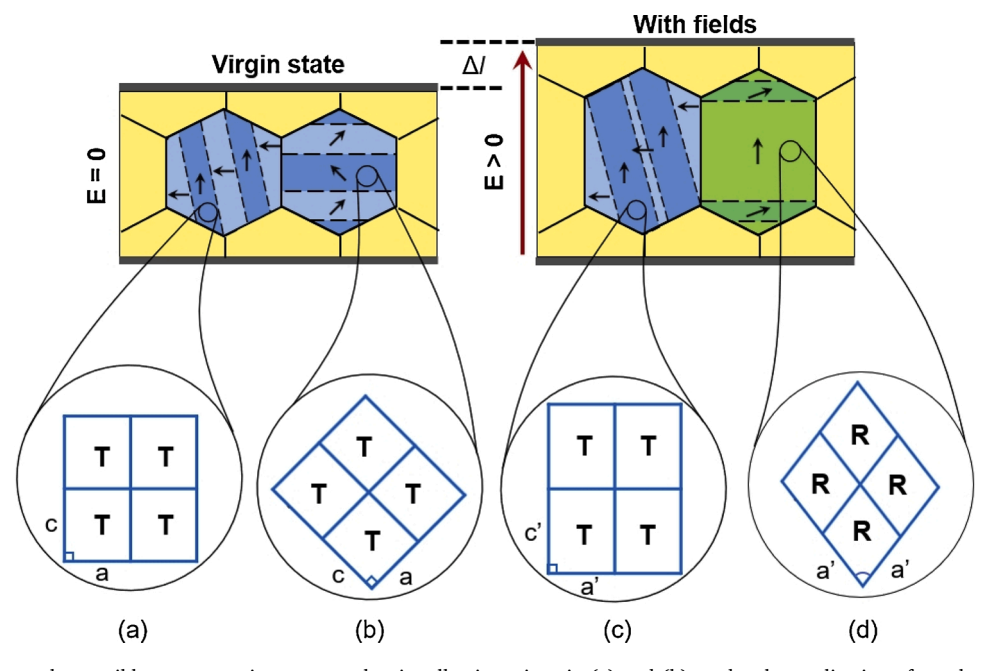


Fig. 5. At the virgin state, the possible representative tetragonal unit cell orientations in (a) and (b); under the application of an electric field, the elongated tetragonal unit cells in (c) and distorted rhombohedral-like unit cells in (d).

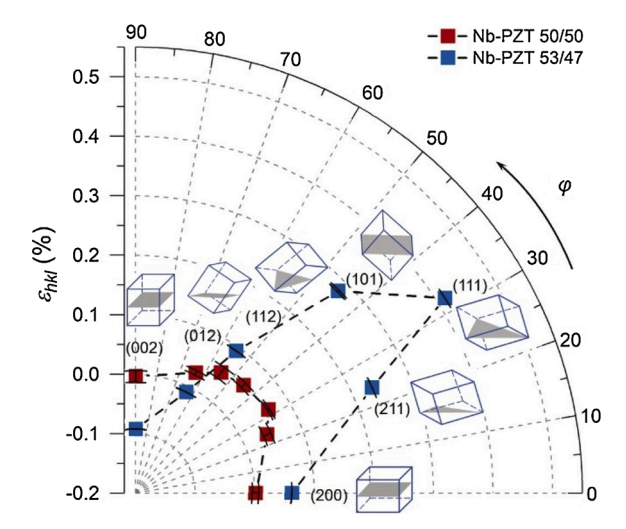


Fig. 6. Orientation-dependent, field-induced lattice strains parallel to the field direction in Nb-PZT 50/50 and Nb-PZT 53/47 under a macroscopic electric field of 3 kV/mm.

crystallographic orientations in which the 002 pole is parallel to the electric field, i.e., the tetragonal c-axis. Likewise, the data point for (111) represents 111 lattice strains in crystallographic orientations in which the 111 pole is parallel to the electric field. The schematic tetragonal unit cell models in Fig. 6 represent the crystallographic orientations in real space, with the (hkl) plane perpendicular to the electric field direction. The figure illustrates that both compositions exhibit the highest field-induced lattice strain in orientations in which the 111 pole is parallel to the electric field direction, and the lowest strain in orientations in which the 002 pole is parallel to the electric field direction. However, while orientations in which the 002 poles are parallel to the electric field direction exhibit relatively small strains, these orientations are aligned such that they are favorable for domain wall motion rather than lattice distortion. The orientations with 111 poles closely aligned to the electric field direction are more favorably oriented for lattice strain rather than domain wall motion. Moreover, to accommodate a large deformation strain in the polycrystalline aggregate, the orientations with 111 poles closely aligned to the field direction are also shown to exhibit transitions from the tetragonal to rhombohedral phases.

While we have utilized the orientations in which 002 and 111 poles are parallel to the electric field to illustrate representative cases, the polycrystalline material consists of all possible crystallographic orientations and the anisotropic phase transition can be studied in this full orientation space. Esteves et al. presented a simple variant-selection mechanism model based entirely on geometry (i.e., no energetics) for initially randomly-oriented ferroelectric polycrystalline materials under a saturating electric field [11]. The simulated result based on 20,000 randomly oriented crystals is illustrated in an inverse pole figure shown in Fig. 7. With a saturating electric field applied parallel to a given specimen dimension, crystals oriented with a 001 pole parallel to the field direction remain in the tetragonal phase, whereas the rhombohedral phase is preferred in crystals oriented with the 111 pole parallel to the electric field direction. This simulation is consistent with the experimental observations in the present work for the near-MPB composition, Nb-PZT 53/47.

5. Conclusions

In summary, we demonstrate an orientation dependence in the electric-field-induced, tetragonal-to-rhombohedral phase transition in Nb-PZT 53/47 piezoceramics, as evidenced by *in situ* synchrotron-based high-energy XRD studies. The phase transition behavior is only observed in compositions nearest the MPB where the two phases are energetically

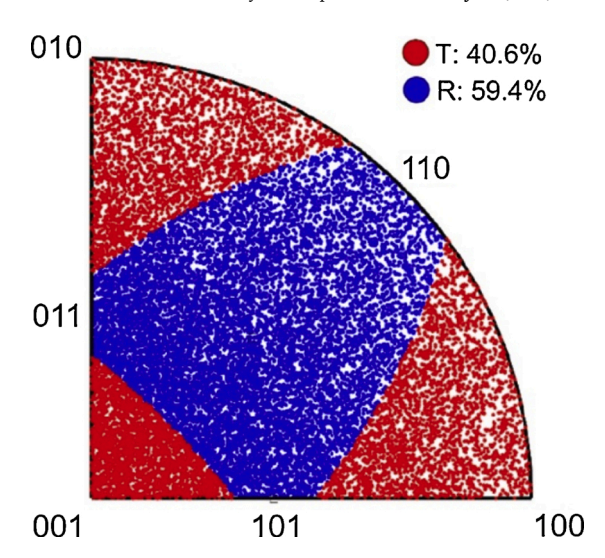


Fig. 7. Inverse pole figure, representing the electric field direction, of a multiphase simulation of tetragonal and rhombohedral grains, and their resulting phase selection based on variant selection. Reproduced from Esteves et al. Acta Mater., vol. 132, pp. 96–105, 2017.

similar, and is shown to be highly anisotropic with a preferential response when the electric field is oriented nearest perpendicular to (*hhh*). The anisotropic nature of the phase transition is only apparent by evaluating all scattering vectors relative to the electric field direction.

Declaration of Competing Interest

The authors declare no conflict of interest.

Acknowledgements

This material is based upon work supported by the National Science Foundation (NSF), as part of the Center for Dielectrics and Piezoelectrics (CDP) under Grant Nos. IIP-1841453 and IIP-1841466. The authors appreciate PI Ceramic for providing ferroelectric materials for study. This work was performed in part at the Analytical Instrumentation Facility (AIF) at North Carolina State University, which is supported by the State of North Carolina and the National Science Foundation (NSF award number ECCS-2025064). The AIF is a member of the North Carolina Research Triangle Nanotechnology Network (RTNN), a site in the National Nanotechnology Coordinated Infrastructure (NNCI). This research used resources of the Advanced Photon Source, a U.S. Department of Energy (DOE) Office of Science User Facility operated for the DOE Office of Science by Argonne National Laboratory under Contract No. DE-AC02-06CH11357.

Appendix A. Supplementary data

Supplementary material related to this article can be found, in the online version, at doi:https://doi.org/10.1016/j.jeurceramsoc.2021.0 1.043.

References

- D. Damjanovic, Contributions to the piezoelectric effect in ferroelectric single crystals and ceramics, J. Am. Ceram. Soc. 88 (10) (2005) 2663–2676.
- [2] Q.M. Zhang, W.Y. Pan, S.J. Jang, L.E. Cross, Domain wall excitations and their contributions to the weak-signal response of doped lead zirconate titanate ceramics, J. Appl. Phys. 64 (11) (1988) 6445–6451.
- [3] M.J. Hoffmann, M. Hammer, A. Endriss, D.C. Lupascu, Correlation between microstructure, strain behavior, and acoustic emission of soft PZT ceramics, Acta Mater. 49 (7) (2001) 1301–1310.
- [4] J.E. Daniels, W. Jo, J. Rödel, J.L. Jones, Electric-field-induced phase transformation at a lead-free morphotropic phase boundary: Case study in a 93%

- $(Bi_{0.5}Na_{0.5})TiO_3-7\%BaTiO_3$ piezoelectric ceramic, Appl. Phys. Lett. 95 (3) (2009) 03.05
- [5] J.L. Jones, M. Hoffman, J.E. Daniels, A.J. Studer, Direct measurement of the domain switching contribution to the dynamic piezoelectric response in ferroelectric ceramics, Appl. Phys. Lett. 89 (9) (2006) 1–4.
- [6] A. Pramanick, D. Damjanovic, J.E. Daniels, J.C. Nino, J.L. Jones, Origins of electromechanical coupling in polycrystalline ferroelectrics during subcoercive electrical loading, J. Am. Ceram. Soc. 94 (2) (2011) 293–309.
- [7] M. Hinterstein, et al., Structural description of the macroscopic piezo- and ferroelectric properties of lead zirconate titanate, Phys. Rev. Lett. 107 (7) (2011) 10–13.
- [8] C.C. Chung, C.M. Fancher, C. Isaac, J. Nikkel, E. Hennig, J.L. Jones, Temperature dependence of field-responsive mechanisms in lead zirconate titanate, J. Am. Ceram. Soc. 100 (9) (2017) 4352–4361.
- [9] T. Iamsasri, G. Tutuncu, C. Uthaisar, S. Wongsaenmai, S. Pojprapai, J.L. Jones, Electric field-induced phase transitions in Li-modified Na_{0.5}K_{0.5}NbO₃ at the polymorphic phase boundary, J. Appl. Phys. 117 (2) (2015), 024101.
- [10] J.L. Jones, et al., Domain wall and interphase boundary motion in a two-phase morphotropic phase boundary ferroelectric: Frequency dispersion and contribution to piezoelectric and dielectric properties, Phys. Rev. B - Condens. Matter Mater. Phys. 86 (2) (2012) 1–9.
- [11] G. Esteves, C.M. Fancher, S. Röhrig, G.A. Maier, J.L. Jones, M. Deluca, Electric-field-induced structural changes in multilayer piezoelectric actuators during electrical and mechanical loading, Acta Mater. 132 (2017) 96–105.
- [12] S.E. Park, T.R. Shrout, Ultrahigh strain and piezoelectric behavior in relaxor based ferroelectric single crystals, J. Appl. Phys. 82 (August 4) (1997) 1804–1811.
- [13] M.K. Durbin, E.W. Jacobs, J.C. Hicks, S.E. Park, In situ x-ray diffraction study of an electric field induced phase transition in the single crystal relaxor ferroelectric, 92% Pb(Zn_{1/3}Nb_{2/3})O₃-8% PbTiO₃, Appl. Phys. Lett. 74 (May 19) (1999) 2848-2850.

- [14] J.L. Jones, E.B. Slamovich, K.J. Bowman, Domain texture distributions in tetragonal lead zirconate titanate by x-ray and neutron diffraction, J. Appl. Phys. 97 (3) (2005) 1–6.
- [15] J.L. Jones, E.B. Slamovich, K.J. Bowman, D.C. Lupascu, Domain switching anisotropy in textured bismuth titanate ceramics, J. Appl. Phys. 98 (10) (2005) 0–8.
- [16] M. Hinterstein, et al., Interplay of strain mechanisms in morphotropic piezoceramics, Acta Mater. 94 (2015) 319–327.
- [17] H. Simons, J.E. Daniels, A.J. Studer, J.L. Jones, M. Hoffman, Measurement and analysis of field-induced crystallographic texture using curved position-sensitive diffraction detectors, J. Electroceramics 32 (4) (2014) 283–291.
- [18] J.E. Daniels, A. Pramanick, J.L. Jones, Time-resolved characterization of ferroelectrics using high-energy X-ray diffraction, IEEE Trans. Ultrason. Ferroelectr. Freq. Control 56 (8) (2009) 1539–1545.
- [19] Computergestützte Multiskalenmodellierung Zur Virtuellen Entwicklung Polykristalliner Ferroelektrischer Materialien (COMFEM). Report, 2010.
- [20] C. Zhao, et al., Deconvolved intrinsic and extrinsic contributions to electrostrain in high performance, Nb-doped Pb(ZrxTi1-x)O3piezoceramics (0.50 \leq x \leq 0.56), Acta Mater. 158 (2018) 369–380.
- [21] A.P. Hammersley, S.O. Svensson, M. Hanfland, A.N. Fitch, D. Hausermann, Twodimensional detector software: From real detector to idealised image or two-theta scan, High Press. Res. 14 (4–6) (1996) 235–248.
- [22] L. Fan, J. Chen, Y. Ren, Z. Pan, L. Zhang, X. Xing, Unique Piezoelectric Properties of the Monoclinic Phase in Pb (Zr,Ti) O3 Ceramics: Large Lattice Strain and Negligible Domain Switching, Phys. Rev. Lett. 116 (2) (2016) 1–5.
- [23] H. Liu, et al., Role of Reversible Phase Transformation for Strong Piezoelectric Performance at the Morphotropic Phase Boundary, Phys. Rev. Lett. 120 (5) (2018) 1–19
- [24] J.L. Jones, et al., Time-resolved and orientation-dependent electric-field-induced strains in lead zirconate titanate ceramics, Appl. Phys. Lett. 90 (17) (2007) 23–25.